Published in final edited form as:
Free Radic Biol Med. 2008 February 15; 44(4): 682–691. doi:10.1016/j.freeradbiomed.2007.10.056.

Assessment of wound-site redox environment and the significance of Rac2 in cutaneous healing

Navdeep Ojha, **Sashwati Roy**, **Guanglong He**[¶], **Sabyasachi Biswas**, **Murugesan Velayutham**[¶], **Savita Khanna**, **Periannan Kuppusamy**[¶], **Jay L. Zweier**[¶], and **Chandan K. Sen**

Laboratory of Molecular Medicine, Davis Heart and Lung Research Institute, The Ohio State University Medical Center, Columbus, Ohio 43210

[¶] Departments of Surgery and Internal Medicine, Davis Heart and Lung Research Institute, The Ohio State University Medical Center, Columbus, Ohio 43210

Abstract

We have previously reported that H_2O_2 is actively generated by cells at the wound-site and that H_2O_2-driven redox signaling support wound angiogenesis and healing. In this study, we have standardized a novel and effective electron paramagnetic resonance (EPR) spectroscopy based approach to assess the redox environment of dermal wound site in vivo. Rac2 regulates reduced NADPH oxidase activation and other functional responses in neutrophils. Using Rac2-deficient mice we sought to investigate the significance of Rac2 in wound site redox environment and healing responses. Non-invasive measurements of metabolism of topically applied nitroxide ^{15}N-perdeuterated tempone in murine excisional dermal wounds demonstrated that the wound site is rich in oxidants, the level of which peaks two day post-wounding in the inflammatory phase. Rac2-deficient mice had 3-fold lower production of superoxide compared to controls in similar wounds. In these mice, lower wound-site superoxide level was associated with compromised wound closure. Immunostaining of wound edges harvested during the inflammatory phase showed that the number of phagocytic cells recruited at the wound site in Rac2 deficient and control mice were similar, but the amount of lipid peroxidation was significantly lower in Rac2 deficient mice indicating compromised NADPH oxidase activity. Taken together, the findings of this study support that the wound-site is rich in oxidants. Rac2 significantly contributes to oxidant production at the wound site and supports the healing process.

INTRODUCTION

Disrupted vasculature limits the supply of oxygen to the wound site. Compromised tissue oxygenation or wound hypoxia is viewed as a major factor that limits the healing process as well as wound disinfection [1]. The general consensus has been that, at the wound site, oxygen fuels tissue regeneration [2] and that oxygen-dependent respiratory burst is a primary mechanism to resist infection [3]. Recent works from our laboratory have developed a new paradigm supporting that oxygen-derived reactive species at the wound site not only disinfect the wound but directly contribute to facilitate the healing process [4–7].

Corresponding Author: Prof. Chandan K. Sen, 512 Davis Heart & Lung Research Institute, 473 West 12th Avenue, The Ohio State University Medical Center, Columbus, Ohio 43210, Tel. 614 247 7658, Fax 614 247 7818, E-mail: chandan.sen@osumc.edu.

Wound healing commences with blood coagulation followed by infiltration of neutrophils and macrophages at the wound site to release reactive oxygen species (ROS) by oxygen-consuming respiratory burst. In 1999, the cloning of mox1 (later named as Nox1) marked a major progress in categorically establishing the presence of distinct nicotinamide adenine dinucleotide phosphate (NADPH) oxidases in non-phagocytic cells [8]. Taken together, the wound-site has two clear sources of ROS: *(i)* transient delivery of larger amounts by respiratory burst of phagocytic cells; and *(ii)* sustained delivery of lower amounts by enzymes of the Nox/Duox family present in cells such as the fibroblasts, keratinocytes and endothelial cells [5]. Recent studies show that, at low concentrations, ROS may serve as signaling messengers in the cell and regulate numerous signal transduction and gene expression processes [9]. Inducible ROS generated in some non-phagocytic cells are implicated in mitogenic signaling [10]. A direct role of NADPH oxidases and ROS in facilitating angiogenesis has been proven [4]. In line with these observations we have previously reported that at the wound site, ROS may promote wound angiogenesis by inducing VEGF expression in wound-related cells such as keratinocytes and macrophages [6]. In this study, we employed electron paramagnetic resonance (EPR) spectroscopy and spin trapping to assess wound-site redox environment [11] and to develop an understanding of the role of Rac2-dependent oxidant production [12] in wound healing.

MATERIALS AND METHODS

Chemicals

^{15}N-PDT (4-oxo-2,2,6,6-tetramethylpiperidine-d_{16}-1-oxyl, CDN Isotopes, Quebec, Canada) was used as the nitroxide spin probe. At low concentration (<2 mM), ^{15}N-PDT produces a well-separated doublet EPR spectrum with a hyperfine-coupling constant of 2.2 mT. At higher concentrations, there is spin-spin broadening which causes the two peaks to merge into one broad middle peak of lower amplitude. ^{15}N-PDT provides for enhanced sensitivity and a narrower line-width than non-isotope enriched tempone. The nitroxide solution was prepared at 50 mM concentration in phosphate-buffered saline, sub-aliquoted, and kept frozen until use.

Copper, zinc–superoxide dismutase (SOD1) and catalase were obtained from Sigma Chemical Co. (St. Louis, Mo) and were of the purest grade available. Diethylenetriaminepentaacetic acid (DTPA) and 2,2,6,6-tetramethyl-1-piperidinyloxy (TEMPO) were obtained from Aldrich. Purified 5,5-dimethyl-1-pyrroline-N-oxide (DMPO) was obtained from Dojindo Laboratories (Kumamoto, Japan). Sources of other chemicals used are mentioned as they appear in the text.

Excisional dermal wound model

C57BL/6 mice between the ages of 8–10 weeks were used. Punch biopsy (3 mm) wounds were developed on the back of mice in pairs (Fig. 1A) for L-band EPR experiments. The back of the mouse was shaved with standard animal hair clippers (#40 blade) and disinfected with betadine (Fisher, USA). Using micro-dissecting forceps (Roboz Inc., Maryland), skin of the animal was lifted along the line as shown and a 3 mm dermal biopsy punch (Miltex Inc., USA) was driven through the two folds of skin. Axially, the wounds were made just above the bridge of the back to avoid motion artifacts during EPR measurements This resulted in two symmetrical full thickness 3 mm diameter wounds in mouse without any underlying tissue damage. The separation between the two wounds was kept between 10–15 mm. A similar technique was used to create 8 mm punch wounds for X-band EPR spin trapping experiments.

For wound closure experiment, two 8 mm X 16 mm full-thickness excisional wounds [6] were placed on the dorsal skin, equidistant from the midline and adjacent to the four limbs. Digital photographs of wounds in full view and in one plane were taken with a digital camera on

specified days after wounding. Images were transferred to a computer and wound areas were calculated using the WoundMatrix software [4].

EPR spectroscopy instrumentation for measurements in wound

EPR spectroscopy experiments were performed on an L-band spectrometer (Magnettech GmbH, Germany) which was set up for topical measurements on the skin of mice. A surface coil resonator of 10 mm diameter with automatic tuning and matching control was used. Mice were anesthetized with an intra-peritoneal injection of ketamine (90 mg/kg) and xylazine (20 mg/kg) and placed in prone position between the poles of the magnet. Position of the animal was adjusted to place the surface resonator around the wound and in contact with the skin. After tuning and matching the system, 6 μl of 50 mM PDT was topically applied to the wound site and EPR spectroscopy measurements were started. Measurements were taken for a minimum of 45 minutes or till the nitroxide EPR signal decayed completely, whichever was later. EPR spectroscopy parameters were chosen as follows: Center field 44.4 mT, modulation amplitude 0.0135 mT, scan width 0.81 mT, scan time 20 s, microwave power 25 mW, time constant 0.1 s.

EPR spectra for spin trapping were recorded using quartz flat cells at room temperature with a Bruker ESP 300E spectrometer operating at X-band with 100 kHz modulation frequency and a TM_{110} cavity. DMPO (50 μl of 1 M) was topically applied to two day-old 8 mm punch biopsy wounds. After 10 minutes, the wound rinsate was collected from the wound cavity, diluted 20X in PBS containing DTPA, and its EPR spectra was recorded.

Direct H_2O_2 measurements

H_2O_2 levels in wound fluid were measured using a real-time electrochemical H_2O_2 measurement as described [13]. The Apollo 4000 system (WPI, Sarasota, FL) was used for analysis. H_2O_2 was measured using the ISO-HPO-2 2.0 mm stainless steel sensor, with replaceable membrane sleeves and an internal refillable electrolyte. This electrode technology includes a H_2O_2 sensing element and separate reference electrode encased within a single Faraday-shielded probe design (WPI, Sarasota, FL). Wound fluid was harvested from mice and was immediately used for direct H_2O_2 measurement as reported [4].

EPR data acquisition and analysis

EPR spectra were acquired and stored using the *Analysis* software (Magnettech GmbH.). The data was then converted into a special format that was read using custom-built software in our laboratory for visualization, analysis and export of spectral parameters (*e.g.* intensity and line-width) into Microsoft Excel, where the final decay curves of the nitroxide were generated. Table Curve 2D software was used for mathematical modeling of nitroxide kinetics.

Quantitation of X-band EPR spectra was performed using custom-built software developed in our laboratory. Quantitation of the observed free radical signals was performed by computer simulation of the spectra and comparison of the double integral of the observed signal with that of a TEMPO standard (1 μM) measured under identical conditions [14].

Histology

Immunohistochemistry—Wounds developed with a 3 mm biopsy punch were collected on day 1 and day 2 using a 6 mm biopsy punch and embedded in OCT. Cryosections (10 μm) were cut and fixed in ice-cold acetone for 5 minutes. Peroxidase blocking was done by incubating the section with 0.3% H_2O_2 for 5 minutes prior to serum-blocking with 10% goat serum. Primary antibody incubations were done as follows: anti-mouse neutrophil (Serotec), 1:100 for 1 hour at room temperature; rabbit anti-HNE (Alexis), 1:500 for 1 hour at room

temperature; rat anti-mouse F4/80, 1:50 for 1 hour at room temperature. Color was developed after incubating the section with the appropriate biotinylated secondary antibody (1:200) utilizing the ABC/DAB method (Vector) according to the manufacturers instructions. Sections were counterstained with hematoxylin, dehydrated sequentially in alcohol with two changes of xylene and mounted with permanent mount.

Immunofluorescence—Two-day old 3 mm punch biopsy wounds, including the wound edge, were harvested with a 6 mm punch biopsy. Skin tissue was embedded in Optimal Cutting Temperature (OCT) compound and frozen. Sections (10 μm) were cut with a cryostat and fixed in acetone. Subsequently sections were blocked with 10% goat serum before incubating with rabbit anti-Hydroxynonenal (1:500; Alexis) and rat anti-mouse neutrophil (1:100; Serotec) together for one hour at room temperature. After washing, the sections were incubated in anti-mouse IgG conjugated to Alexa 488 and anti rat IgG conjugated to Alexa 568 for 30 min at room temperature (both 1:100). Sections were counterstained with DAPI (1:10,000) and visualized under a Zeiss Axiovert 200M microscope.

For CD31 staining, cryosections were fixed in acetone and blocked with 10% BSA Fraction V (Acros) for 30 minutes. Sections were then incubated with PE conjugated anti-mouse CD31 (1:100; eBiosciences) overnight at 4°C, counterstained with DAPI, and visualized as above.

Computer Assisted Image Analysis—A color subtractive-computer assisted image analysis system was used to quantitatively label and calculate immunostained area after staining and subsequent digital imaging [15]. We employed Adobe Photoshop 6.0 with Image Processing Toolkit 5.0 (www.reindeergraphics.com) software for image analysis. This method, instead of positive color selection, serially removes all non-specific color from the images using a sequential method of color background removal leaving behind only the positive stain on a white background. To remove sampling error caused by imaging only a part of the stained tissue, each tissue slide was imaged in three different areas at 20X magnification on a Zeiss microscope. Images were converted from the Zeiss ZVI format to standard JPEG format and loaded into Adobe Photoshop for analysis.

All steps involved in image analysis were stored in a macro in Adobe Photoshop. The macro was developed on an image selected at random from the images of the tissue sections. First, a copy of the layer containing the tissue section image was initially made. The color subtraction routine as described before [15] was modified as required for our images and executed on this new layer. Purple-pink stain of hematoxylin and other background color was colorimetrically removed and replaced with white, leaving behind a dark brown DAB color which was the positive stain. The color subtraction process was continued till all non-specific color was removed from the image. The color subtraction layer was then duplicated and binary thresholding was performed on it. A threshold level of 252 was used. The thresholding routine converts all darker pixels above selected threshold level to black, and all pixels lighter than that to white. This results in a black and white image with positively stained areas in black on a white background. Feature measurement was then performed on this thresholded image to objectively calculate the area of stained tissue as a percentage of the complete image. The macro recording was then stopped, and the macro was saved. This macro is instrumental to generate immunostained areas from all sections automatically and efficiently without user bias.

Statistical analysis

All results are expressed as mean ± SD. The data were analyzed and compared using ANOVA and Student's t-test where appropriate for statistical significance. Differences between means at $p < 0.05$ were considered significant.

RESULTS

Nitroxide kinetics in wound

Using a non-invasive EPR-based technique we sought to quantify the oxidant concentration at the wound site in mice during the inflammatory phase, which lasts for about 2–3 days after wounding [16]. A nitroxide probe was topically applied to the open wound. Signal decay of the probe applied to the wound was monitored to generate a mathematical model to derive oxidant levels at the wound site. The nitroxide solution was topically applied to the dermal wounds (Fig. 1A) of mice and the resonator placed directly above and around the wound site (Fig. 1B). EPR spectroscopy measurements performed immediately after wounding were collected as a function of time, and are shown in Fig. 1C. At the beginning, one broad peak was observed (0 min). This broad signal is attributed to electron spin exchange interaction of the nitroxide radicals in the concentrated solution at the surface of the skin [17]. With time, the broad central peak became narrower and weaker. In addition, another component with two sharp peaks (doublet) appeared, increased over the first 10 min and then gradually declined because of reduction of nitroxide. Only the left peak is shown here in Fig. 1C, as the two side peaks were symmetrical. This component is a result of the diluted ^{15}N-PDT within the tissue which gives rise to a doublet with hyperfine-coupling constant a_N = 2.2 mT [18].

Oxidant levels at wound site peak 2 days after wounding

To estimate the level of oxidants at wound site in the inflammatory phase of wound healing, the above-described EPR measurements were performed on day 0, day 1 and day 2 after wounding because the inflammatory phase in wounds lasts from day 0 to day 3 in mice [16]. Nitroxide half-life was calculated as $0.693/k_r$. Figure 1F shows the change in half-life of nitroxide at the wound site with healing. It is known that the stability of a probe in a tissue characterizes the level of oxidants present at that location [18]. We observed that subsequent to wounding, the stability of nitroxide probe at the wound site is higher (Fig. 1D). Thus, a higher concentration of oxidants was evident at the wound site on day 2 after wounding, which is the peak time for respiratory burst by the inflammatory cells [16].

Spin trapping of superoxide radical with DMPO

After observing an oxidizing environment at the wound site with the nitroxide clearance approach, we employed DMPO as spin trap to quantitate superoxide radical production *in vivo*. In the presence of DMPO, EPR analysis of wound rinsate in phosphate-buffered saline containing the metal ion chelator DTPA indicated formation of the spin trap radical adduct DMPO-OH. The spectrum in Fig. 2A, a 1:2:2:1 quartet that is not evident in the absence of wound rinsate (Fig. 2C), exhibited isotropic hyperfine splitting of $a_N = a_H$ = 1.49 mT, characteristic of the hydroxyl radical adduct of DMPO, DMPO-OH. DMPO-OH can be formed by direct trapping of hydroxyl radical by DMPO, or as a product of decomposition of the superoxide radical adduct DMPO-OOH [19,20]. DMPO-OOH, with a half time of 45 s in aqueous media, decomposes into a number of products, including DMPO-OH [21]. The abolishment of the DMPO-OH spectrum by the addition of superoxide dismutase (SOD1) (Fig. 2B), further suggests that the DMPO-OH adduct is derived from superoxide. Thus, we concluded that the DMPO-OH spectrum noted at the wound site in our studies was caused by superoxide, the direct product of NADPH oxidases [5].

Next, we investigated the time course of superoxide generation at the wound site following wounding. Fig. 3 shows EPR spectra of wound rinsate collected at specific time-points after wounding. We noted that superoxide production was at its maximum on day 2 when the inflammatory cells are actively engaged in respiratory burst activity. Quantitation of superoxide at the wound site is shown in Fig. 3F, where the data is normalized to show relative

concentrations. This corroborates our data on nitroxide decay (Fig. 1F) showing higher oxidant levels at wound site two days after wounding.

Impaired healing and compromised superoxide production in Rac2 knockout mice

NADPH oxidase deficiency impairs wound healing as is noted in chronic granulomatous disease [5]. Defect in the expression of any of the essential subunits of NADPH oxidase *e.g.*, Rac2 is expected to compromise respiratory burst dependent oxidant production [22]. We noted that $Rac2^{-/-}$ mice suffer from significantly delayed wound closure (Fig. 4) indicating that Rac2-dependent NADPH oxidase activity is important in supporting wound healing. EPR spectra of wound rinsate collected from wild type and $Rac2^{-/-}$ mice 2 days after wounding is shown in Fig. 5A and B, respectively. We chose this time point because the amount of superoxide production at the wound site in wild type animals was found to be highest at day 2 (Fig. 1F, Fig. 3F). We observed a three-fold decrease in superoxide production at the wound site in $Rac2^{-/-}$ mice compared to wild type (Fig. 5C). Quantitation of H_2O_2 in wound fluid using the electrochemical detection system showed significantly decreased peroxide concentration in wound fluid in $rac2^{-/-}$ mice compared to matched wild-type (Fig. 5D).

$Rac2^{-/-}$ mice: recruitment of phagocytic cells to wound site is not affected, but their function is impaired

When skin is wounded, the local tissue rapidly recruits inflammatory cells. Neutrophils reach the wound site in hours followed by macrophages which peak in day 2 after wounding [23]. We examined the wound-edge tissue from $Rac2^{-/-}$ mice and their corresponding wild-type mice. The number of neutrophils recruited to the wound-edge tissue on day 2 was imaged and scored using a color subtractive-computer assisted image analysis method. Two days after wounding, $Rac2^{-/-}$ mice tended to recruit more neutrophils to the wound-site but the difference was not statistically significant ($p = 0.07$, Fig. 6). Consistent with the pattern noted for neutrophils, macrophage recruitment in $Rac2^{-/-}$ mice tended to be higher but the difference was not statistically significant ($p = 0.11$, Fig. 7). Taken together, it can be concluded that $Rac2^{-/-}$ did not compromise the ability of the mice to recruit inflammatory cells to the wound site.

At the wound site, inflammatory cells exhibit potent respiratory burst activity. 4-Hydroxy-2-nonenal (HNE) is a major product of endogenous lipid peroxidation, which is found as a footprint in the aftermath of respiratory burst [24]. 4-HNE levels were clearly lower in the wound-edge tissue of $Rac2^{-/-}$ mice compared to that of wild-type controls (Fig. 8AC). This observation is consistent with other results in this study demonstrating lower levels of reactive oxygen species in the wound of $Rac2^{-/-}$ mice. Employing a double immuno-staining approach it was evident that in wound-edge tissue of wild-type mice neutrophils co-localize with 4-HNE stain indicating active respiratory burst of the inflammatory cells (Fig. 8D). In the wound-edge tissue of $Rac2^{-/-}$ mice, however, neutrophils did not associate with strong 4-HNE stain supporting other data in this study that indicate compromised respiratory burst activity in $Rac2^{-/-}$ mice (Fig. 8E).

Impaired angiogenesis in $Rac2^{-/-}$ mice

$Rac2^{-/-}$ mice suffer from significantly delayed wound closure (Fig. 4) indicating that rac2 is an essential component for wound closure. CD31 is characteristic of endothelial cells. To study role of rac2 in angiogenesis we performed immunohistochemical staining for CD31 (red) and DAPI (blue, nuclei) on cryosectioned wound-edge tissue from wild-type and $rac2^{-/-}$ mice sampled 8 days after wounding (Fig. 9). Compared to wild-type mice, the lower abundance of CD31 stain in the sections obtained from $rac2^{-/-}$ mice (right) suggests impaired endothelial cell proliferation in mice deficient in rac2.

DISCUSSION

NADPH oxidase-dependent superoxide generation is highly active at the wound site [4]. The highest level of peroxide in bodily fluids is found in the wound [4]. At the wound sites, hydrogen peroxide drive wound angiogenesis [4] by inducing redox signaling [9]. Such redox-dependent mechanisms are compromised under conditions of NADPH oxidase deficiency. Thus, individuals with defective NADPH oxidase suffer from impaired healing such as in chronic granulomatous disease [5]. On the other hand, approaches to facilitate NADPH oxidase activity at the wound-site by Rac1 gene delivery promoted wound closure [6]. Rac GTPases, Rac 1 and Rac2, are crucial regulators of NADPH oxidase function in eukaryotic cells [12]. In this work, using nitroxyl spin probe ^{15}N-PDT we observed that a healing wound is significantly rich in oxidants two days after wounding, which corresponds to the inflammatory phase. Lower stability of the probe corresponds to a more reductive state, and a higher stability corresponds to a more oxidative state of the wound tissue. This work presents first evidence demonstrating the production of superoxide radicals at the wound site using a DMPO spin trapping technique. Basal superoxide production in the intact skin was below detection limits. Superoxide levels, however, sharply increased as a function of time. Superoxide levels were the highest at day two of healing which corresponds with the peak time of respiratory burst of invading phagocytes [4]. We have previously developed instrumentation and methodology for non-invasive measurement and imaging of nitroxide spin labels in the skin of normal human volunteers [18]. This work represents a maiden effort to employ L-band and X-band EPR for quantitative measurement of redox status and spin trapping of superoxide radicals in full thickness dermal wounds in mice.

Rac2 is a Rho GTPase that is expressed in cells of hematopoietic origin, including neutrophils and macrophages. Rac2 regulates reduced NADPH oxidase activation and other functional responses in neutrophils. Although not required for translocation of p47phox and p67phox, Rac2 is necessary for optimal activity of the assembled oxidase complex [22]. Mice deficient in hematopoietic-specific Rac2 exhibit agonist-specific defects in neutrophil functions including superoxide production elicited by phorbol ester, fMLP, or IgG-coated particles, despite expression of the highly homologous Rac1 isoform. Although Rac2 is a relatively minor isoform in murine macrophages, it plays a non-overlapping role with Rac1 to regulate host defense functions in this phagocyte lineage [22]. Consistent with these observations we noted that Rac2$^{-/-}$ mice suffer from impaired oxidant production at the wound site. EPR results showed that in Rac2 deficient mice oxidant production during the inflammatory phase was 3-fold lower than that in corresponding wild-type control mice. Lower level of oxidants, under conditions of Rac2 deficiency, was associated with impaired wound closure. Rac2 deficiency has been reported in humans and is associated with poor wound healing [25]. In humans, Rac2 plays a critical and unique role to maintain normal neutrophil function [8].

Rac GTPases are believed to contribute to migration in leukocytes by transducing signals from cell surface receptors to the actin and microtubule cytoskeletons. Mammals have three closely related Rac isoforms, Rac1, Rac2 and Rac3, and it is widely assumed that cell migration requires the activity of these Rac GTPases. Rac1 and Rac2 have distinct roles in regulating cell morphology, migration and invasion, but are not essential for macrophage migration or chemotaxis [26]. Consistent with this observation we noted that a lower level of oxidants at the wound site in Rac2$^{-/-}$ mice was not caused because of impaired level of recruitment of phagocytic cells. The recruitment of both macrophages and neutrophils to the wound site was not impaired in Rac2$^{-/-}$ mice. Taken together, the findings of this study support that the wound-site is rich in oxidants. Rac2 significantly contributes to oxidant production at the wound site and supports the healing process.

Acknowledgments

Supported by NIH-RO1 GM069589 and GM077185 to CKS.

References

1. Gordillo GM, Sen CK. Revisiting the essential role of oxygen in wound healing. Am J Surg 2003;186:259–263. [PubMed: 12946829]
2. Kivisaari J, Vihersaari T, Renvall S, Niinikoski J. Energy metabolism of experimental wounds at various oxygen environments. Annals of Surgery 1975;181:823–828. [PubMed: 1138632]
3. Greif R, Akca O, Horn EP, Kurz A, Sessler DI. Supplemental perioperative oxygen to reduce the incidence of surgical-wound infection. Outcomes Research Group.[see comment]. New England Journal of Medicine 2000;342:161–167. [PubMed: 10639541]
4. Roy S, Khanna S, Nallu K, Hunt TK, Sen CK. Dermal wound healing is subject to redox control. Mol Ther 2006;13:211–220. [PubMed: 16126008]
5. Sen CK. The general case for redox control of wound repair. Wound Repair Regen 2003;11:431–438. [PubMed: 14617282]
6. Sen CK, Khanna S, Babior BM, Hunt TK, Ellison EC, Roy S. Oxidant-induced vascular endothelial growth factor expression in human keratinocytes and cutaneous wound healing. J Biol Chem 2002;277:33284–33290. [PubMed: 12068011]
7. Sen CK, Khanna S, Gordillo G, Bagchi D, Bagchi M, Roy S. Oxygen, oxidants, and antioxidants in wound healing: an emerging paradigm. Annals of the New York Academy of Sciences 2002;957:239–249. [PubMed: 12074976]
8. Suh YA, Arnold RS, Lassegue B, Shi J, Xu X, Sorescu D, Chung AB, Griendling KK, Lambeth JD. Cell transformation by the superoxide-generating oxidase Mox1. Nature 1999;401:79–82. [PubMed: 10485709]
9. Stone JR, Yang S. Hydrogen peroxide: a signaling messenger. Antioxid Redox Signal 2006;8:243–270. [PubMed: 16677071]
10. Irani K, Xia Y, Zweier JL, Sollott SJ, Der CJ, Fearon ER, Sundaresan M, Finkel T, Goldschmidt-Clermont PJ. Mitogenic signaling mediated by oxidants in Ras-transformed fibroblasts. Science 1997;275:1649–1652. [PubMed: 9054359]
11. Schafer FQ, Buettner GR. Redox environment of the cell as viewed through the redox state of the glutathione disulfide/glutathione couple. Free Radic Biol Med 2001;30:1191–1212. [PubMed: 11368918]
12. Hordijk PL. Regulation of NADPH oxidases: the role of Rac proteins. Circ Res 2006;98:453–462. [PubMed: 16514078]
13. Liu X, Zweier JL. A real-time electrochemical technique for measurement of cellular hydrogen peroxide generation and consumption: evaluation in human polymorphonuclear leukocytes. Free Radic Biol Med 2001;31:894–901. [PubMed: 11585708]
14. Velayutham M, Villamena FA, Navamal M, Fishbein JC, Zweier JL. Glutathione-mediated formation of oxygen free radicals by the major metabolite of oltipraz. Chem Res Toxicol 2005;18:970–975. [PubMed: 15962931]
15. Underwood RA, Gibran NS, Muffley LA, Usui ML, Olerud JE. Color subtractive-computer-assisted image analysis for quantification of cutaneous nerves in a diabetic mouse model. J Histochem Cytochem 2001;49:1285–1291. [PubMed: 11561013]
16. Beanes SR, Dang C, Soo C, Ting K. Skin repair and scar formation: the central role of TGF. Expert Rev Mol Med 2003;2003:1–22. [PubMed: 14987411]
17. Sachse JH, Marsh D. Line intensities in spin-exchanged nitroxide ESR spectra. J Magn Reson 1986;68:540–543.
18. He G, Samouilov A, Kuppusamy P, Zweier JL. In vivo EPR imaging of the distribution and metabolism of nitroxide radicals in human skin. J Magn Reson 2001;148:155–164. [PubMed: 11133289]
19. Finkelstein E, Rosen GM, Rauckman EJ, Paxton J. Spin trapping of superoxide. Mol Pharmacol 1979;16:676–685. [PubMed: 229403]

20. Roubaud V, Sankarapandi S, Kuppusamy P, Tordo P, Zweier JL. Quantitative measurement of superoxide generation and oxygen consumption from leukocytes using electron paramagnetic resonance spectroscopy. Anal Biochem 1998;257:210–217. [PubMed: 9514781]

21. Rosen GM, Pou S, Ramos CL, Cohen MS, Britigan BE. Free radicals and phagocytic cells. Faseb J 1995;9:200–209. [PubMed: 7540156]

22. Yamauchi A, Kim C, Li S, Marchal CC, Towe J, Atkinson SJ, Dinauer MC. Rac2-deficient murine macrophages have selective defects in superoxide production and phagocytosis of opsonized particles. J Immunol 2004;173:5971–5979. [PubMed: 15528331]

23. Witte MB, Barbul A. General principles of wound healing. Surg Clin North Am 1997;77:509–528. [PubMed: 9194878]

24. Esterbauer H, Schaur RJ, Zollner H. Chemistry and biochemistry of 4-hydroxynonenal, malonaldehyde and related aldehydes. Free Radic Biol Med 1991;11:81–128. [PubMed: 1937131]

25. Ambruso DR, Knall C, Abell AN, Panepinto J, Kurkchubasche A, Thurman G, Gonzalez-Aller C, Hiester A, deBoer M, Harbeck RJ, Oyer R, Johnson GL, Roos D. Human neutrophil immunodeficiency syndrome is associated with an inhibitory Rac2 mutation. Proc Natl Acad Sci U S A 2000;97:4654–4659. [PubMed: 10758162]

26. Wheeler AP, Wells CM, Smith SD, Vega FM, Henderson RB, Tybulewicz VL, Ridley AJ. Rac1 and Rac2 regulate macrophage morphology but are not essential for migration. J Cell Sci 2006;119:2749–2757. [PubMed: 16772332]

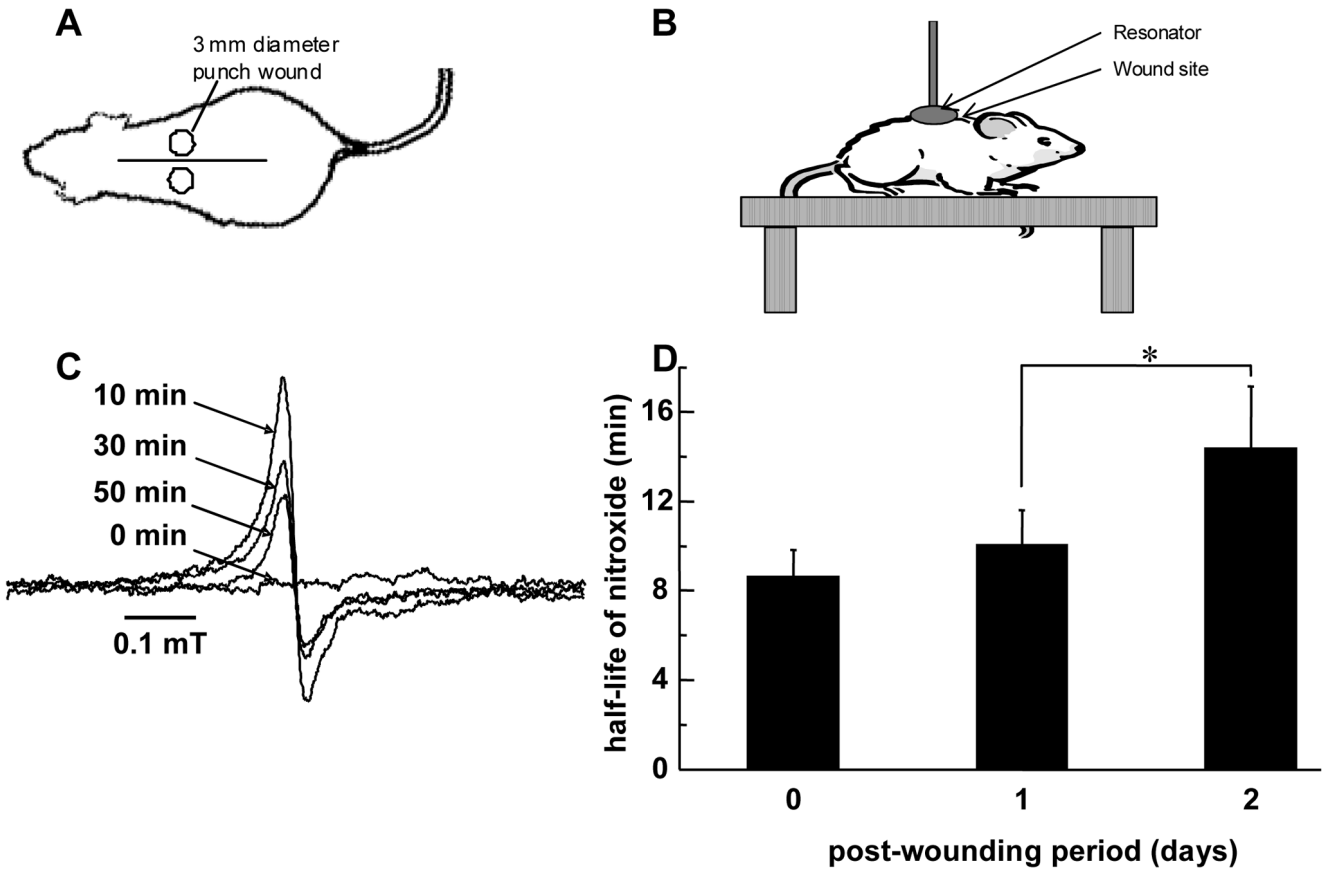

Figure 1.

Topical EPR spectroscopy of wounds. (A) Mouse sketch with a pair of 3 mm full thickness dermal punch wounds (not drawn to scale). The distance between the wounds was 10–15 mm. These wounds were made above the bridge of the back so as to avoid motion artifacts caused by breathing while EPR spectroscopy measurements were being done. (B) The mouse was anesthetized and placed on a height adjustable table which allows exact positioning of resonator above and around wound site. (C) Time course of EPR spectra of ^{15}N-PDT after topical application to wound. The spectra were taken at L-band using a surface resonator. A 6 μl solution of 50 mM PDT was applied to wound site and spectral acquisitions were immediately started. Data acquisition parameters were as stated in the text. At the beginning of experiment the left and right peaks (only left peak shown here) were non-existent. With time, these peaks appear and increase in intensity, and then gradually decline. (D) Oxidant level at wound site increases 2 days after wounding. 3 mm punch biopsy wounds were made on back of C57BL/6 mice. 6 μl of 50 mM ^{15}N-PDT was topically applied on the wound and EPR spectra were immediately started. EPR spectra maxima of left peak were used to generate decay curves which were mathematically fitted and half life was calculated. Measurements were taken from the same wound on day 0, day 1 and day 2 after wounding. Data is shown as mean ± SD, n = 6, * indicates $p < 0.05$.

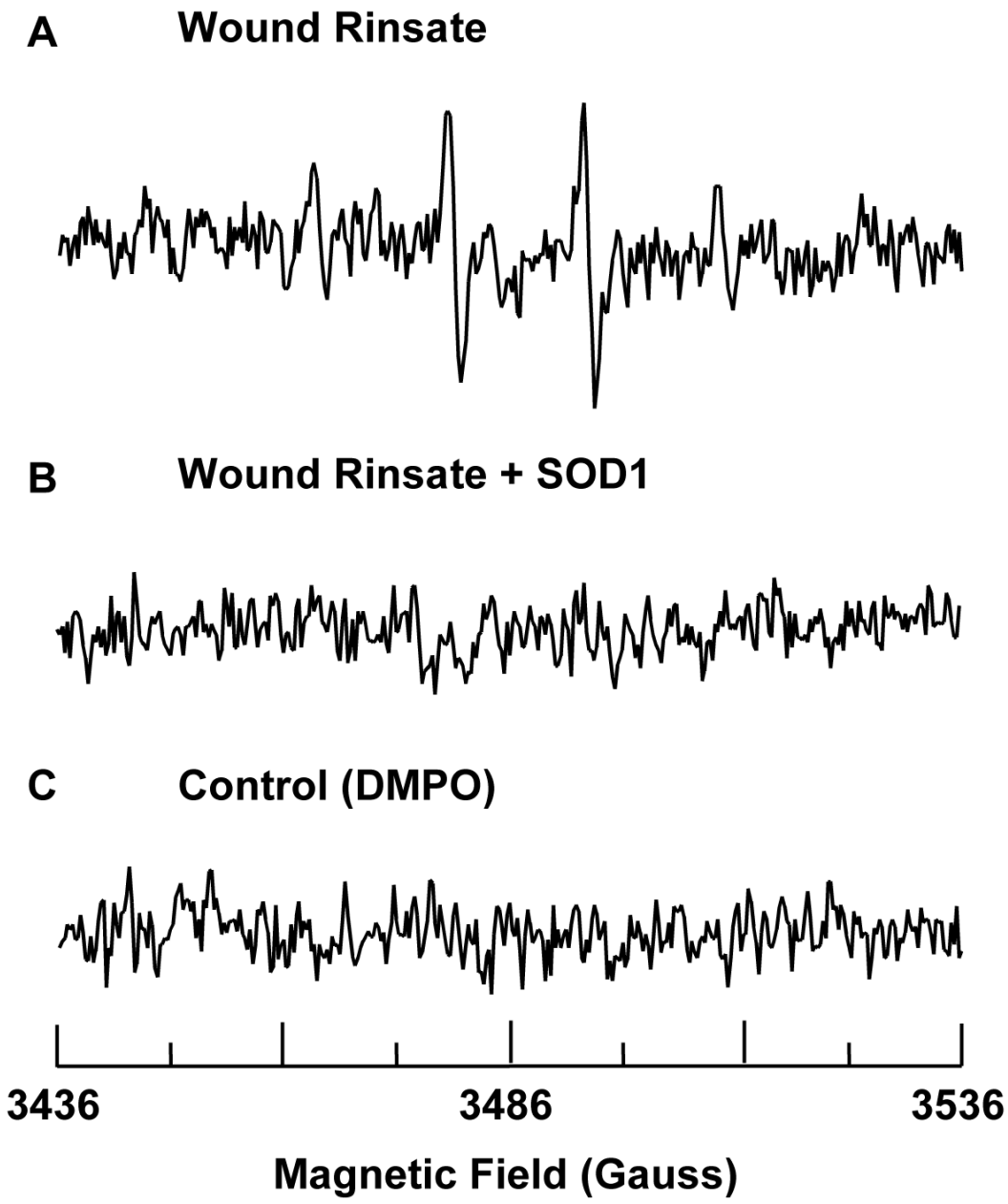

Figure 2.

Presence of superoxide at wound site. (A) The spectra shows presence of spin adduct DMPO-OH in wound rinsate. 50 μl of 1 M DMPO was topically applied to 2 days old 8 mm punch biopsy wounds. After 10 minutes wound rinsate was collected from the wound cavity, diluted 20X in PBS containing DTPA, and its EPR spectrum was recorded. (B) 5 μl of SOD1 (300 μM) was topically applied to the wound 10 minutes before application of DMPO and subsequent collection of wound rinsate. Addition of SOD1 quenches the EPR signal indicating that the source of signal is from superoxide. (C) Spectrum of DMPO in PBS. X-band EPR measurements were carried out using a quartz flat cell at room temperature. EPR instrument parameters used were as follows: microwave frequency 9.77 GHz; modulation frequency 100

kHz; modulation amplitude 1 G; microwave power 20 mW; number of scans 30; scan time 30 s; and time constant 81 ms.

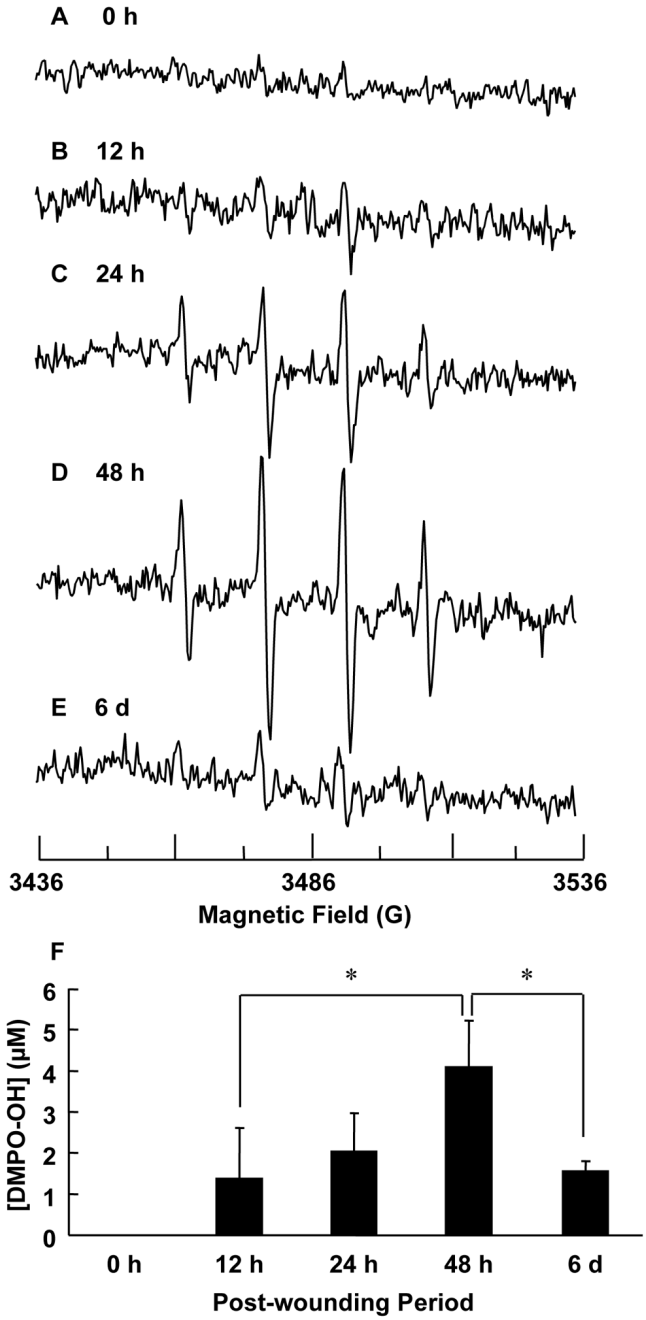

Figure 3.

Superoxide production at wound site peaks 2 days after wounding as measured from DMPO spin adduct taken from wound rinsate. EPR measurements were carried out as described before. X-band EPR spectra was recorded from wound rinsate collected at various time points as shown: (A) 0 hour, (B) 12 hour, (C) 24 hour, (D) 48 hour, and (E) 6 day. Clearly the maximum signal is obtained 48 hours after wounding. (F) Quantitation of DMPO-OH spin adduct formation in wound rinsate normalized to maximum intensity observed on day 2 after wounding. Quantitation was performed by computer simulation of the spectra and comparison of double integral of observed signal with that of a TEMPO standard (1 μM) measured under

identical conditions. The increased production of superoxide correlates with the respiratory burst of inflammatory cells, which peaks at day 2 post wounding. n = 3, * indicates $p < 0.05$.

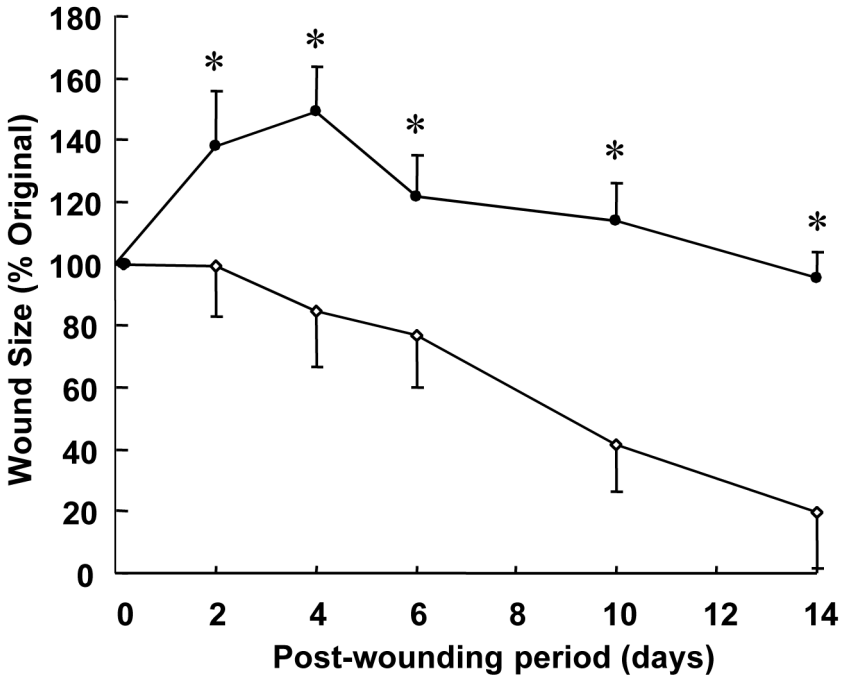

Figure 4.

Slow wound healing response of Rac2$^{-/-}$ animals. Two 8 mm X 16 mm full thickness dermal wounds were created on backs of Rac2$^{-/-}$ (filled circles) and wild type (open circles) mice. Digital Photographs of wounds in full view and in one plane were taken with a digital camera (Sony Mavica) on specified days after wounding. Wound areas were calculated using WoundMatrix software. * indicates $p < 0.05$, $n = 4$ in each group.

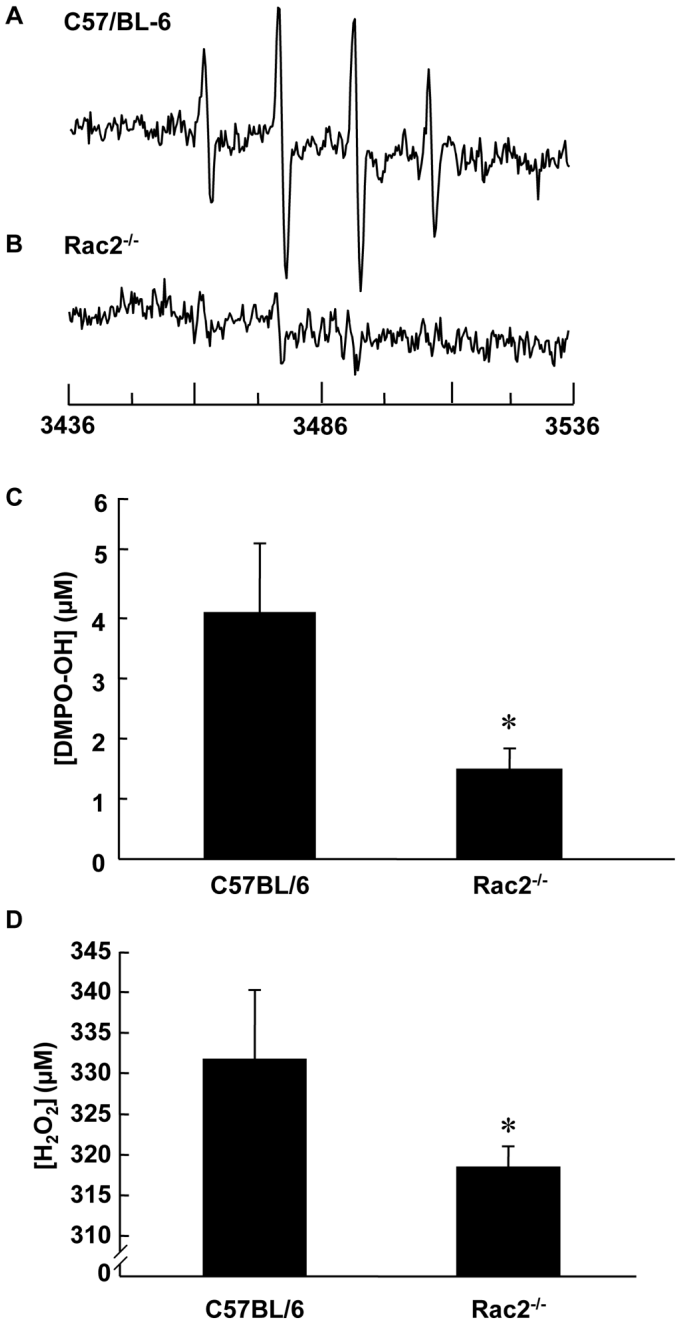

Figure 5.

Decreased superoxide production at wound site in Rac2$^{-/-}$ mouse corresponds to slow healing response of animals. (A) EPR measurements were done as described in the text at day 2 after wounding in wild type and Rac2$^{-/-}$ mice. (A) and (B) show X-band EPR spectra of wound rinsate in PBS from wild type and Rac2$^{-/-}$ mice, respectively. (C) Quantitation of DMPO-OH production in wild type and Rac2$^{-/-}$ mice, indicating that a much lower amount of superoxide is produced in Rac2$^{-/-}$ mice given the compromised NADPH oxidase system in phagocytic cells. For this experiment, n = 3 in each group. (D) H_2O_2 concentration in wound fluid. Hunt–Schilling cylinders were implanted in each of five 8 to 10-week old C57BL/6 and Rac2$^{-/-}$ mice. On day 2, fluid was collected. 200 mM NaN_3 was added to inhibit peroxidase activity.

To discern the H_2O_2- sensitive component of the signal detected in wound fluid 0.03 ml of the azide-free fluid was treated with 350 units of catalase. The catalase-sensitive component was interpreted as H_2O_2. Standard curve was generated using authentic H_2O_2 tested for UV absorbance. Data is shown as mean ± SD, n = 5 in each group, * indicates $p < 0.05$.

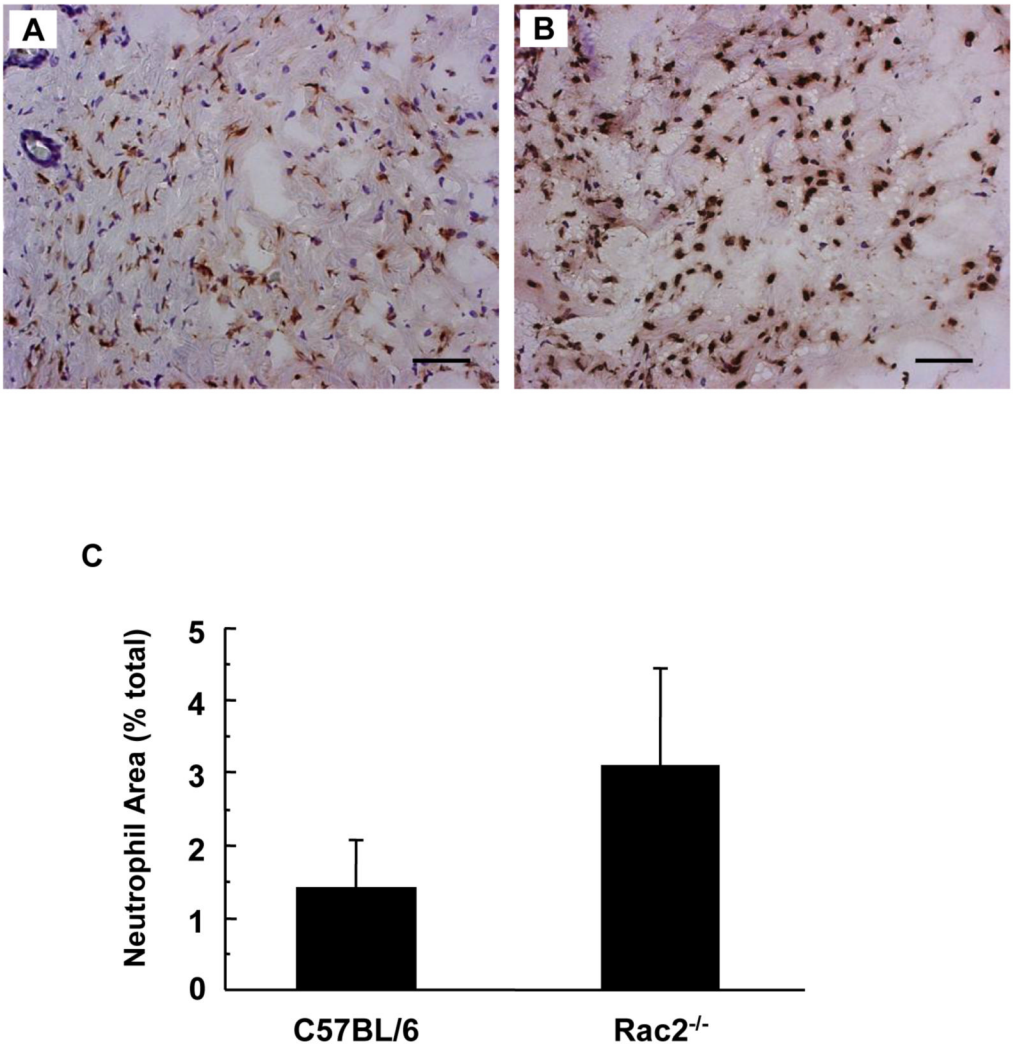

Figure 6.

Neutrophil recruitment to wound-site is increased in $Rac2^{-/-}$ mice. Neutrophil staining of C57BL/6 mice (A) and $Rac2^{-/-}$ mice (B) was performed on frozen sections of regenerated skin at the wound-site sampled 2 days after wounding. (C) Bar graph representing image analysis outcome. Three different regions from each wound were imaged on a microscope and analyzed with Adobe Photoshop using a color subtractive-computer assisted image analysis system. $Rac2^{-/-}$ mice show a trend towards higher recruitment of neutrophils to the wound-site compared to wild type, possibly to compensate for the lower NADPH oxidase activity in the neutrophils. All images at 20X magnification, Scale bar = 50 microns, n = 4 in each group.

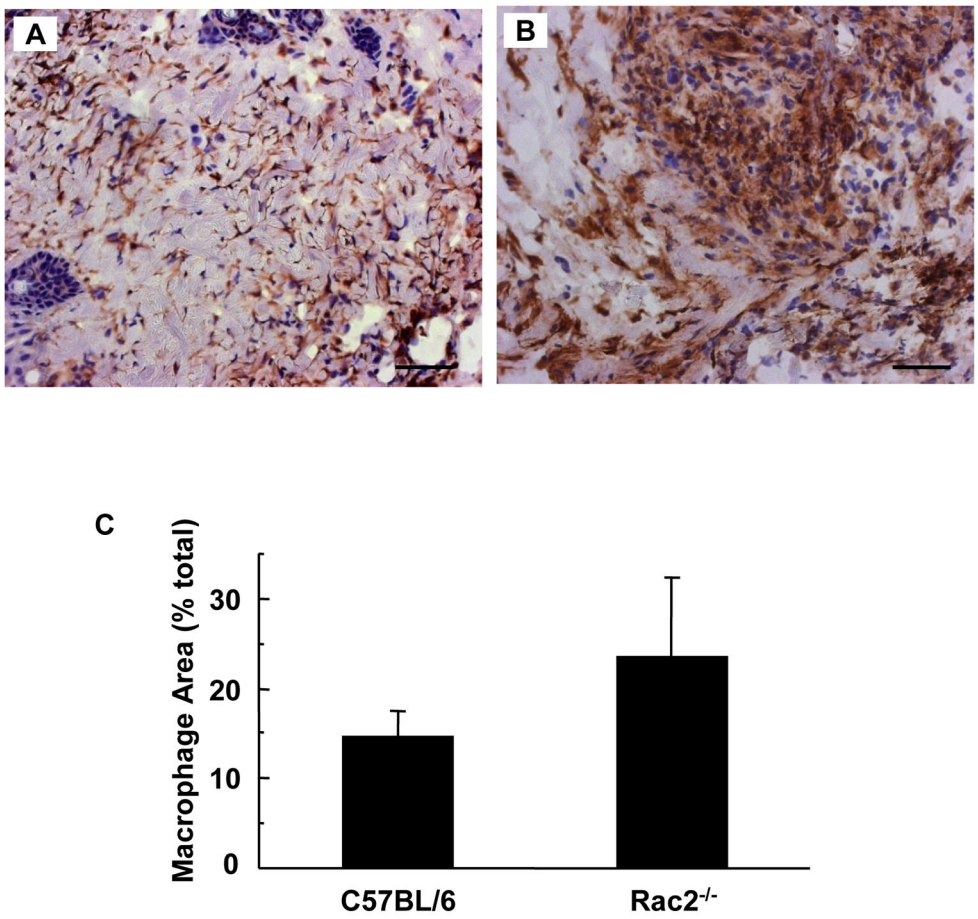

Figure 7.

Macrophage recruitment to wound-site is increased in $Rac2^{-/-}$ mice. F4/80 macrophage staining of C57BL/6 mice (A) and $Rac2^{-/-}$ mice (B) was performed on frozen sections of regenerated skin at the wound-site sampled 2 days after wounding. (C) Bar graph representing image analysis outcome. $Rac2^{-/-}$ shows a trend towards higher recruitment of macrophages to the wound-site compared to wild type. All images at 20X magnification, Scale bar = 50 microns, n = 4 in each group.

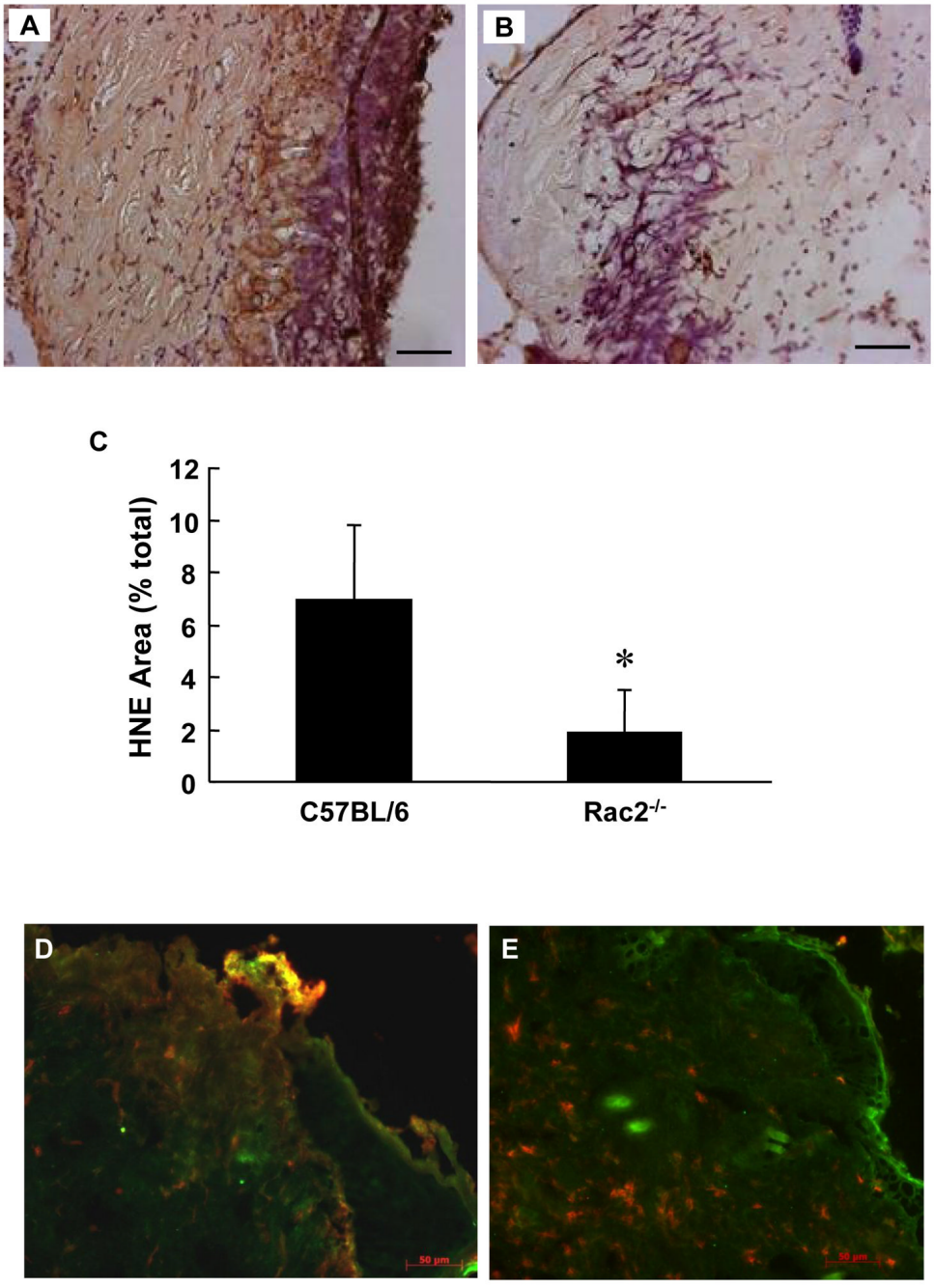

Figure 8.

Lower lipid peroxidation at wound site in $Rac2^{-/-}$ mice. HNE staining was performed on OCT fixed frozen sections of regenerated skin at the wound-site sampled 1 day after wounding. $Rac2^{-/-}$ (B) shows lesser lipid peroxidation indicative of lower (vs. wild type in A) activity of inflammatory cells. (C) Bar graph represents Image Analysis outcome. (D) and (E) Double immunostaining was performed on OCT-fixed frozen sections of regenerated skin at the wound-site sampled 2 days after wounding. Wild type (D) shows higher level (vs. $Rac2^{-/-}$ on right) of co-localization of lipid peroxidation (green) and neutrophils (red) producing an orange/yellow hue all over the section indicating that in $Rac2^{-/-}$ mice neutrophils infiltrate into the wound site but do not cause lipid peroxidation as they lack sufficient NADPH oxidase

activity. All images at 20X magnification, Scale bar = 50 microns. Data is shown as mean ± SD, n = 4 in each group, * indicates $p < 0.05$.

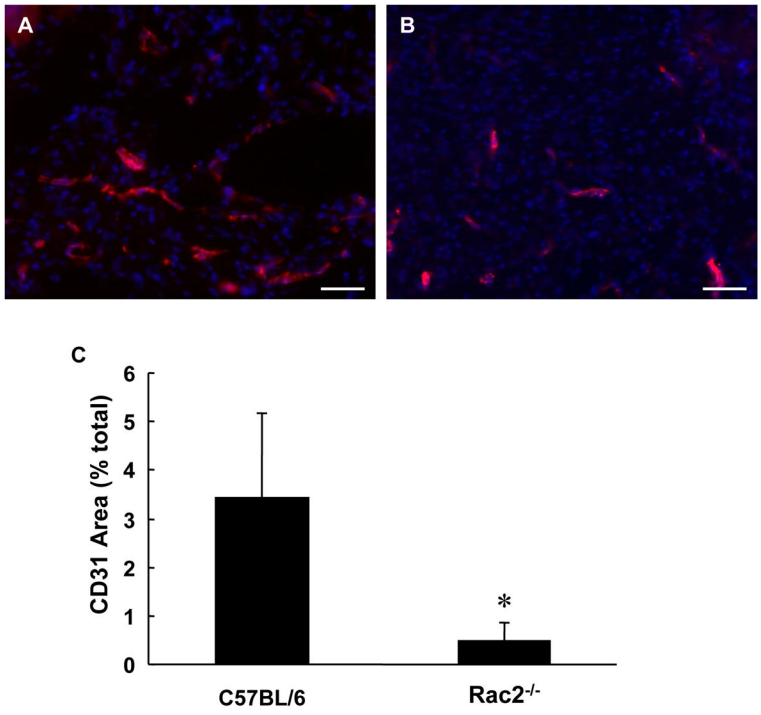

Figure 9.

Impaired angiogenesis Rac2$^{-/-}$ mice. For estimation of vascularization, we performed immunohistochemical staining for CD31(red) and DAPI (blue, nuclei) on cryosectioned wound tissue from wild-type (A) and Rac2$^{-/-}$ mice (B) sampled 8 days after wounding. (C) Bar graph representing image analysis outcome. The higher abundance of CD31 red stain in the section obtained from wild-type mice (left) demonstrates better vascularization and angiogenesis versus Rac2$^{-/-}$ (right). All images at 20X magnification, Scale bar = 50 microns, n = 4 in each group.